

Effects of Microwave Drying on the Cell Wall Structures of Round Bamboo

Huangfei Lv,^{a,#} Shun Yang,^{a,#} Yixin Zhu,^a Xin Shu,^a Wenshi Cao,^a Bin Xu,^{a,*} and Benhua Fei^{b,*}

Effects of microwave irradiation on bamboo cell wall structures were studied. Microwave treatment resulted in samples exhibiting smoother surfaces, deformed parenchyma cells, and increased porosity. Microwave treatment altered microfibril orientation through the formation of hydrogen bonds. The peak at 3440 cm⁻¹, assigned to O-H stretching, decreased. Meanwhile, intermolecular and intramolecular bonds were formed, increasing the uniformity of microfibrils. Condensation reactions in surface hydroxyl groups and the formation of intramolecular hydroxyl groups in the amorphous region under microwave irradiation also improved the fiber arrangement uniformity. After treatment, the HCH and HOC bonds were reduced and the ester bonds were broken down. The methoxy and aromatic ring hydroxyl groups were oxidized, as indicated by the increase in the absorption peak at 148 ppm. The hydroxyl groups in the amorphous region near the fiber surface decreased, as did hemicellulose content, but there was an increase in secondary crystalline fibers.

DOI: 10.15376/biores.18.2.4071-4084

Keywords: Round bamboo; Microwave drying; Cell wall; Structural properties

Contact information: a: College of Forest and Landscape, Anhui Agricultural University, Hefei, China, 230036; b: International Centre for Bamboo and Rattan, Beijing, China, 100102; *Corresponding authors: feibenhua@icbr.ac.cn; xubin@ahau.edu.cn; #Co-author: The authors contributed equally to this work.

INTRODUCTION

Bamboo is an abundant natural resource that plays an important role in human society (Jiang 2007). As a structural material, bamboo has many advantageous traits, such as ease of large-scale cultivation, rapid growth and high strength, flexibility, and toughness. Most engineered structural applications employ pristine round bamboo, which is composed of hollow cylindrical shoots separated by solid transversal diaphragms at nodes.

Bamboo is composed mainly of fiber cells and parenchyma cells and has a highly complex wall structure compared to wood cells (Wang *et al.* 2014). The secondary wall of bamboo is a complex multi-layered structure with continuous thin and thick layers arranged alternately, and there can be more than 10 layers (Parameswaran and Liese 1976). The layered wall structures of bamboo vary among species and positions, and they change as the bamboo grows and develops (Khalil *et al.* 2012). As a natural biomass, bamboo stems are primarily composed of cellulose, hemicellulose, and lignin. Cellulose is formed of linear macromolecules with a double-helical conformation formed by glucose monomers *via* glycosidic bonds, bonds which can be broken under acidic conditions, leading to degradation (Grantham *et al.* 2017). Hemicellulose is made mainly of xylan with molecular side chains of arabinose and glucuronic acid. Hemicellulose has a certain amount of branched chains, and the molecular chains contain numerous free hydroxyl groups, giving

the bamboo an increased water absorption capacity in a humid environment. Similarly, lignin transitions to a glassy state and is partly degraded under the appropriate hydrothermal conditions, resulting in an altered cell morphology and even cracks in parts of the cell wall (Wang *et al.* 2017; Shen *et al.* 2019).

Bamboo has a high moisture content (45% to 90%), so it needs immediate drying after harvesting to avoid microbial damage and to make it ready for storage, processing, and utilization. To date, the industrial applications of round bamboo have been limited by the lack of reasonable drying methods. Notably, drying is a key step in industrial bamboo use, and the current common drying technologies (*e.g.* air drying and kiln drying) can require high amounts of energy, produce large amounts of environmental pollution, and be very time consuming (Prasad and Pandey 2012). Hence, a simple, fast, efficient, and clean drying technology is greatly needed to improve the industrial processing and utilization of bamboo.

Round bamboo has a concave-convex structure in which a hollow cylindrical rod is divided into multiple segments. Bamboo walls are rich in parenchyma cells, are highly hygroscopic, and bamboo shrinks below the fiber saturation point when dry (Prasad and Pandey 2012). All these factors make it difficult to dry round bamboo to produce a quality product. The main factor limiting its development is the lack of drying technology. Round bamboo drying is an important process in its industrial application. The drying characteristics refer to the effects of drying methods on properties (Shen 2020; Yan *et al.* 2022). Recently, microwave drying has become a promising process in biomass industries. It offers many advantages compared to conventional heating. The treated round bamboo can affect the composite state and binding boundary of cell wall substances, leading to differences in fiber plasticization (Elbaum 2007; Zhang 2017; Kang *et al.* 2019).

Microwave drying is a promising biomass processing alternative because it offers many advantages compared to conventional heating. The basic principle of microwave drying is the dipolar polarization mechanism. Polar molecules vibrate at high speeds; thus friction between polar molecules and the environment occurs (Anita *et al.* 2020). Microwave irradiation heats the entire volume of the material so that all parts rapidly obtain heat and increase their temperature simultaneously, resulting in a shorter processing time, higher uniformity and selectivity, higher monosaccharide stability, and less energy input than conventional heating methods (Mood *et al.* 2013; Tsubaki *et al.* 2013). Moreover, microwave drying has no direct waste product. Microwave drying has been applied to improve enzymatic hydrolysis efficiency in biomass (Fatriasari *et al.* 2017). However, few studies have been conducted on how microwave drying alters bamboo stem cell wall structures. Considering the low efficiency and poor quality control of traditional drying methods, this study applied the microwave drying method to round bamboo using the representative bamboo species *Phyllostachys iridescens* C.Y.Yao & S.Y.Chen. The impact of microwave drying on the wall structures and the distributions and variability of the main chemical components of round bamboo were investigated.

EXPERIMENTAL

Materials and Methods

The four-year-old Hong bamboo (*Phyllostachys iridescens* C.Y.Yao & S.Y.Chen) used in this study was harvested from Anhui Province, China. One-meter-long samples were collected from the bamboo stems at a height between 1.5 and 2.5 m above the ground.

Sections with diameters ranging from 30 to 40 mm and wall thicknesses ranging from 3 to 4 mm were collected from the bamboo stems. The sections were treated using microwave irradiation equipment at 80 °C until the moisture content reached to 10%, and the operational power was kept at 6 kW and the frequency at 2450 MHz. The treatment was monitored using a digital control unit in the dryer. The tray was connected to a loading cell with a precision of 0.03%. After drying, the samples were allowed to cool to room temperature. Control samples were treated in convection drying oven at 80 °C.

Wall Structure Properties Observations

Scanning electron microscopy (SEM)

Changes in sample structures were observed using SEM (Hitachi S-4800, Japan). Samples with thicknesses of 5 to 10 mm were dehydrated in a series of ethanol concentrations, sputter-coated with 8 nm of gold for 90 s, and imaged using SEM. The changes produced by the microwave treatment of samples were analyzed.

Pore structure

The changes in pore structure were examined using small angle X-ray scattering (SAXS, NSRL, Hefei) with X-rays produced by a 40 W micro-focused Cu source. The powders of 100 mesh were used for this study. The wavelength $\lambda = 1.54 \text{ \AA}$ was detected using a moveable Pilatus 300 k pixel detector. The angle was 0.08° to 5° and the vector ranged from 0.07 nm^{-1} to 2.1 nm^{-1} .

Atomic force microscopy (AFM)

The AFM method used was based on the protocols in Casdorff *et al.* (2018). Imaging was performed in air using the ‘Tapping Mode’ of a Dimension ICON AFM (Burker, Santa Barbara, CA, USA) under controlled climatic conditions. Imaging was conducted using the software extension NanoScope Analysis 4.0, which performed image processing and data analysis/manipulation to obtain clear images. The non-contact cantilever (RTESP, resonance frequency 321 to 342 kHz, 8 nm silicon probe) was calibrated with the contact-free method for a beam-shaped cantilevers, taking into account the environmental conditions and cantilever dimensions (length 115 to 135 μm , width 30 to 40 μm , thickness 3.5 to 4.5 μm). The measurement parameters were set to the following values: Setpoint, 60 nN; z-length, 50 nm; pixel time, 12 ms; scanning frequency, 0.8 to 1.0 Hz; scanning angle, 0° . This resulted in an extend rate of 340 to 380 kHz (the extend rate controls the speed of the probe tapping). The mapping resolution was set at 512×512 pixels and the scan size was set to $1 \times 1 \mu\text{m}^2$.

Chemical Components Analysis

Fourier transform infrared spectroscopy (FTIR)

The surface chemical properties of samples were observed by FTIR (Bruker Tensor-27, Germany) over the range of 500 to 4000 cm^{-1} at a resolution of 4 cm^{-1} with 32 scans. Radial sections of samples with thicknesses of 10 μm were collected using a sliding microtome. All images with sizes of $120 \times 120 \mu\text{m}^2$ were calculated from the average absorbance in the observed range.

Raman spectroscopy

Raman spectroscopy was conducted according to previously published methods (Felhofer *et al.* 2020; Lv *et al.* 2022). Sections of 10 μm thickness were prepared on a

rotary microtome (Leica SM 2010R, Germany) and mounted on glass slides for Raman imaging. Photographic measurements of the intact vascular portion of the preparation were performed using a laser at a wavelength of 532 nm through an immersion objective (Nikon 100 × NA = 1.4). The measuring range was 120 × 120 μm². After the test, a cosmic ray removal filter was applied and the spectra were baseline corrected in the measurement software. Origin Pro 8.5 was used to analyze the data.

Nuclear magnetic resonance (NMR) spectroscopy

The chemical shifts of samples were determined by CP/MAS13CNMR (Bruker 600M, Germany). Each sample was ground and filtered through 100 mesh into powder. These powders were used for solid-state cross-polarized magic-angle spinning NMR analysis (solid-state CP/MAS13CNMR) at 8000 to 10000 using a 4 mm CP/MAS probe. Spectra were recorded on a Brook ADVANCE NEO400WB spectrometer. The standard pulse sequence was 100.40 MHz (Zhang *et al.* 2021).

RESULTS AND DISCUSSION

Wall Structure

Figure 1 shows images of the wall structure characteristics of the control specimen and the treated sample. This shows that the treatment method had no obvious effect on the morphological characteristics of the bamboo vascular bundles (Fig. 1a and 1d). The fibrils of the microwaved sample showed some deformation in the cavity, and the surface of the cell wall was very smooth (Fig. 1e).

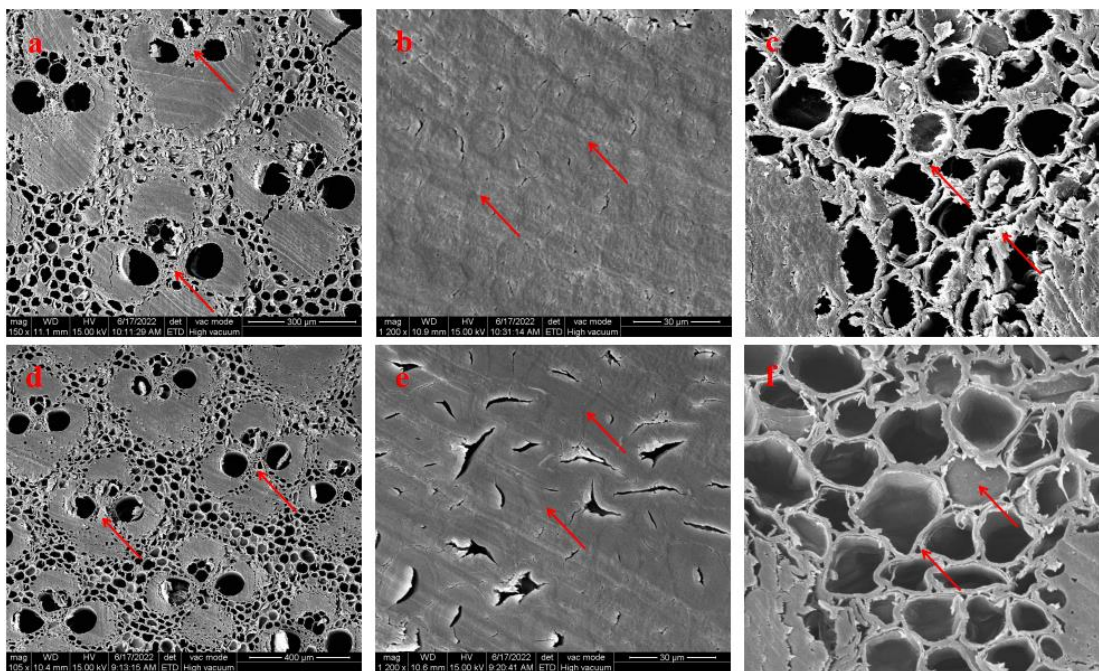


Fig. 1. SEM images of wall structure properties of control and treated sample. a) The vascular bundles of control sample. b) The fiber cells of control samples. c) The parenchyma cells of control sample. d) The vascular bundles of treated sample. e) The fiber cells of treated sample. f) The parenchyma cells of treated sample

In contrast, the pores of the control sample changed significantly (Fig. 1b). In addition, the cell walls of the control group were rougher. After microwave treatment, the parenchyma cells were obviously deformed (Fig. 1f), but the layered depressions on the inner wall were still clearly visible, indicating that microwaving had little effect on the parenchymal cells. At the same time, the parenchymal cell morphology of the control group was profoundly changed (Fig. 1c), with some cells collapsed and the parietal layer changed. Consequently, the overall cell morphology of the treated samples was slightly altered compared to the control samples, resulting in a smoother appearance. These results suggest that microwave treatment is a promising method for drying biomass due to the lower degree of deformation compared with conventional drying.

Pore Structure

Figure 2 shows the small-angle X-ray scattering data of samples after different treatments. The profiles revealed the trends of porous changing (Fig. 2a). Furthermore, it showed that porous structures were enhanced during microwave treatment. This was probably due to the accelerated generation of water vapor under microwave irradiation. The rapid increase in vapor pressure damaged the pits membrane, which not only resulted in higher porosity, but also enlarged the existing pores (Wang *et al.* 2014; Zhou *et al.* 2017). The 2D scattering images showed sharp and clear edges at the tips and boundaries after microwave treatment (Fig. 2b and 2c). This was likely because microwave treatment partially changed the orientations of the microfibrils on the surface of cell wall, especially the parenchyma cells, and resulted in the formation of a large number of hydrogen bonds. The hydrogens bonds were established during dehydration by microwave treatment, and the microfibril orientations were consistent with the cell axis (Chen *et al.* 2021).

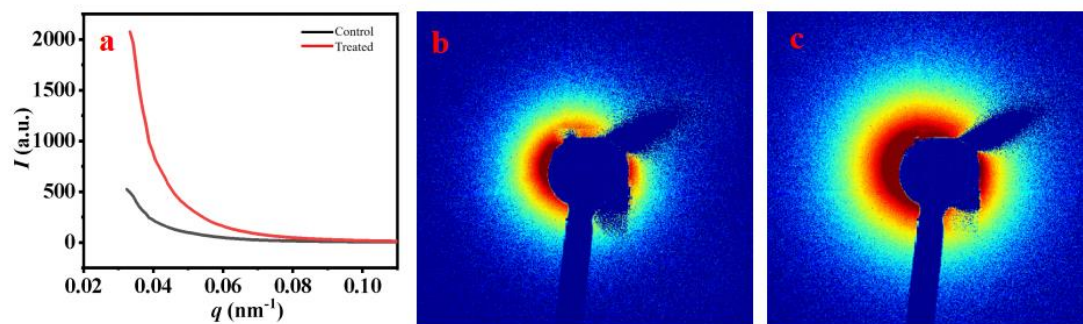


Fig. 2. Small-angle X-ray scattering data of samples. a) The profile of pore structure changing with different treatment. b) The 2D scattering image of control sample. c) The 2D scattering image of treated sample

Atomic Force Microscopy (AFM)

Figure 3 shows the AFM images of the structures of the parenchyma cell walls. The parenchyma cells of bamboo are mainly composed of cellulose, hemicellulose, and lignin. Parenchyma cell walls were very thin compared to fiber cell walls (Fig. 3a and 3d). This played an important role in determining the final cell morphology when the samples were treated with microwave irradiation. The lignin in parenchyma cells adheres to the surfaces of cell walls in reticular form. Under the microwave treatment, the lignin was partially degraded. Furthermore, microwave treatment exposed more microfibrils, which aggregated on the surface of cell wall (Ozgenç *et al.* 2017; Zhang *et al.* 2022). Therefore,

the surface of the treated samples became smoother than the control (Fig. 3b and 3e). Figures 3c and 3f further illustrate these findings. Previous studies have proposed that the cellulose and hemicellulose share van der Waals and hydrogen bonds with each other, which increases stability. Besides, there are many hydroxyl groups on the surface of cell walls (Hanus and Mazeau 2006; Wu 2021). Parenchyma cell walls are composed of varying numbers of oriented microfibril layers, which have an important role in the physical properties of the wall. After treatment, the space taken up by hydroxyl groups was reduced, allowing more hydrogen bonds to be produced. The microfibrils also became more uniform and their crystallinity was increased. Therefore, the mechanical properties of the samples treated by microwave irradiation were increased (Lv *et al.* 2018; Lian *et al.* 2021).

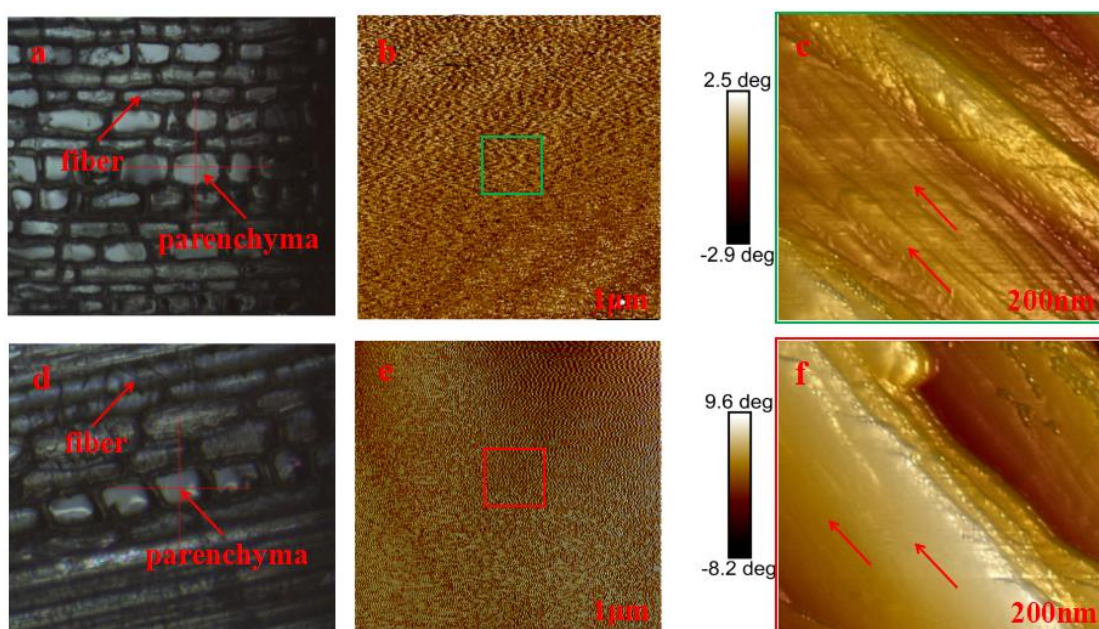


Fig. 3. AFM images and the schematic of the structure of the parenchyma cell wall. a) The test point image of control sample. b,c) The parenchyma cell wall images of control sample. d) The test point image of treated sample. e,f) The parenchyma cell wall images of treated sample.

FTIR Analysis

Figure 4 shows the average FTIR spectra of the samples. It can be seen from the spectrogram (Fig. 4a) that the relative intensity of the peak at 3440 cm^{-1} , which belongs to surface OH stretching, decreased after microwave treatment. This indicated there was a decrease in OH value and a change in the proportional amount of hydrogen bonds in the treated samples. In addition, the peak intensities at 1736 and 1600 cm^{-1} decreased due to the degradation of hemicellulose and the cleavage of the acetyl chain, respectively (Emmanuel *et al.* 2015; Ozgenc *et al.* 2017). In addition, the peaks at 1240 and 1057 cm^{-1} decreased with the decreases in C-O and C-O-C in hemicellulose, respectively (Huang *et al.* 2013). The peak intensity at 1384 cm^{-1} decreased due to reduction in CH bonds in the polysaccharide, indicating that the polysaccharide was degraded after treatment. The peak at 1736 cm^{-1} decreased, indicating that the hemicellulose was partially degraded, reflecting reduced C=O bonds in the hemicellulose acetyl group. There was a clear band at 3200 to 3500 cm^{-1} , which was attributed to the mixture of intermolecular, intramolecular, and free hydrogen bonds with cellulose and water molecules (Kalutskaya and Gusev 1980; Tskaya

and Gvsev 1981; Lin *et al.* 2022; Zhang *et al.* 2022). To further investigate the formation of this hydrogen bond, the 2nd-derivative spectrum was obtained from the band (Fig. 4b). The characteristic peaks of *O6H-O3* molecular hydrogen bonds appeared at 3270 to 3280 cm^{-1} , and the characteristic peaks of *O3H-O5* intramolecular hydrogen bonds and *O2H-O6* intermolecular hydrogen bonds appear at 3400 and 3430 cm^{-1} . After microwave treatment, intermolecular hydrogen bonds formed at 3277 cm^{-1} between the hydroxyl groups of the cellulose chains and between the crystalline regions of the microfibrils (Fig. 4b). This was because during the drying process water evaporates, cell walls shrink, and intermolecular hydrogen bonds form. At the same time, the microfibrils are reorganized in amorphous regions. Furthermore, more intramolecular hydrogen bonds were formed at 3340 cm^{-1} and 3433 cm^{-1} . These hydrogen bonds also promote reorganization of the amorphous regions and aggregation of microfibrils, resulting in higher crystallinity and smoother cell walls (Fig. 3f) (Peng *et al.* 2012; Li *et al.* 2022).

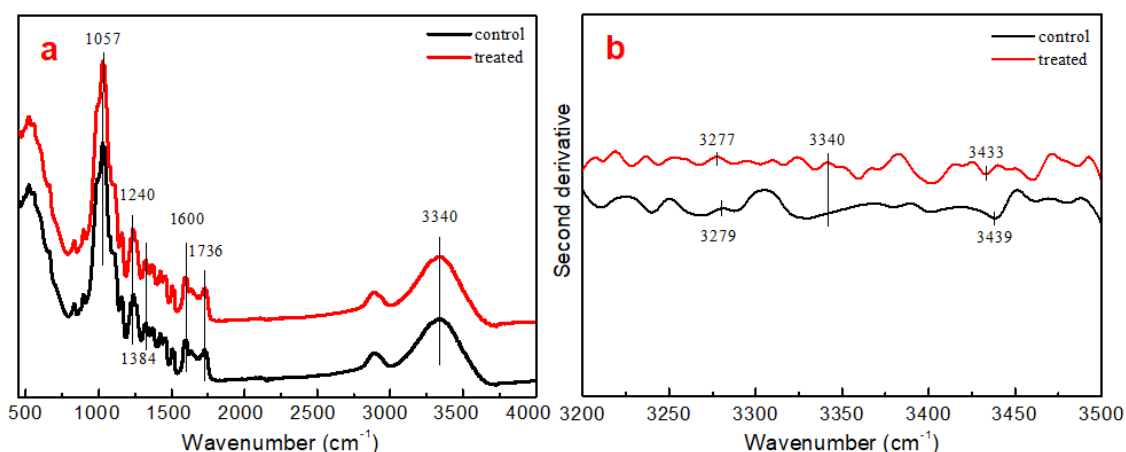


Fig. 4. The average FTIR spectra of samples (a) and the 2nd-derivative of spectra band at 3200 to 3500 cm^{-1} (b).

Raman Analysis

Figure 5 shows the Raman images and spectra of the bamboo samples. In the Raman spectrum (Fig. 5b), the four main peaks at 2940 cm^{-1} , 1600 cm^{-1} , 1450 cm^{-1} , and 1170 cm^{-1} changed to varying degrees after microwave treatment.

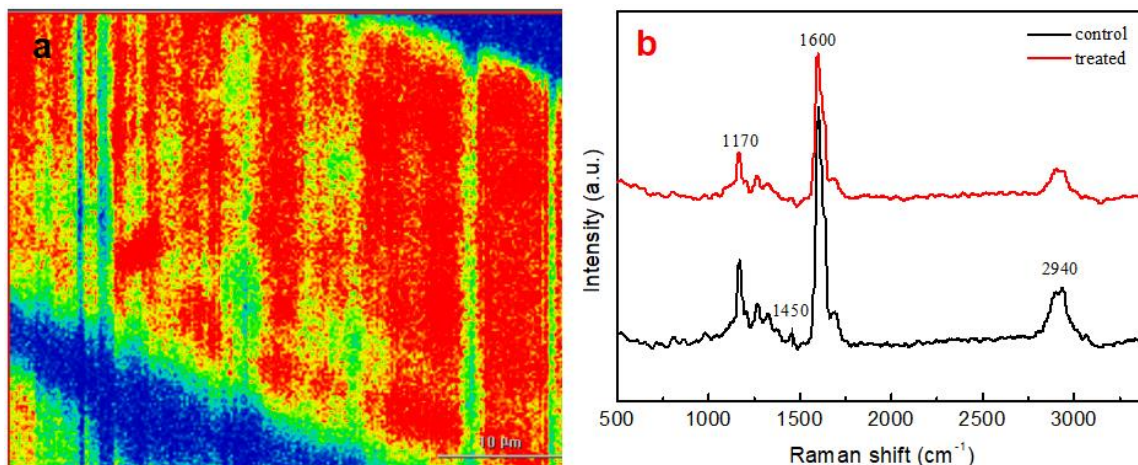


Fig. 5. Raman imaging (a) and spectra (b) of the bamboo samples

These four peaks corresponded to the C-H stretching peaks of cellulose methylamine, the C=C stretching peaks of aromatic lignin rings, the semicircular stretching peaks of benzene or fused benzene rings, and the stretching peaks of carbohydrates (Prats *et al.* 2016; Belt *et al.* 2017; Toscan *et al.* 2017; Bock and Gierlinger 2019). These changes indicated that specific strands or functional groups were cleaved or formed.

The maximum increase was as high as 2940 cm^{-1} for the treated samples. This was mainly due to the condensation reaction of surface hydroxyl groups under microwave conditions, but it was also related to the formation of hydroxyl groups in the amorphous region of the molecule. This indicated there was improved consistency in fiber orientation. At 1600 cm^{-1} , the opposite was true, indicating that the formation of an aromatic scaffold and a more consistent orientation of lignin in the cell wall (Atalla and Agarwal 1985; Schwan *et al.* 1996). The decrease in peak intensity at 1450 cm^{-1} indicated a decrease in the stretching frequency and a decrease in the proportion of HCH and HOC bonds in the aromatic skeleton. Located at 1170 cm^{-1} there is a vibration peak of the complex formed by hydroxycinnamic acid, ester bond and ether bonds, lignin, and hemicellulose. This peak decreased, and the ester bonds were broken by microwave radiation under slightly acidic conditions. Taken together, these results indicated that microwave drying leads to rapid water loss, elevated temperature, partial carbohydrate degradation, and prolonged hydrothermal action, leading to the degradation of the complex. Therefore, the vibration peak at this location was reduced.

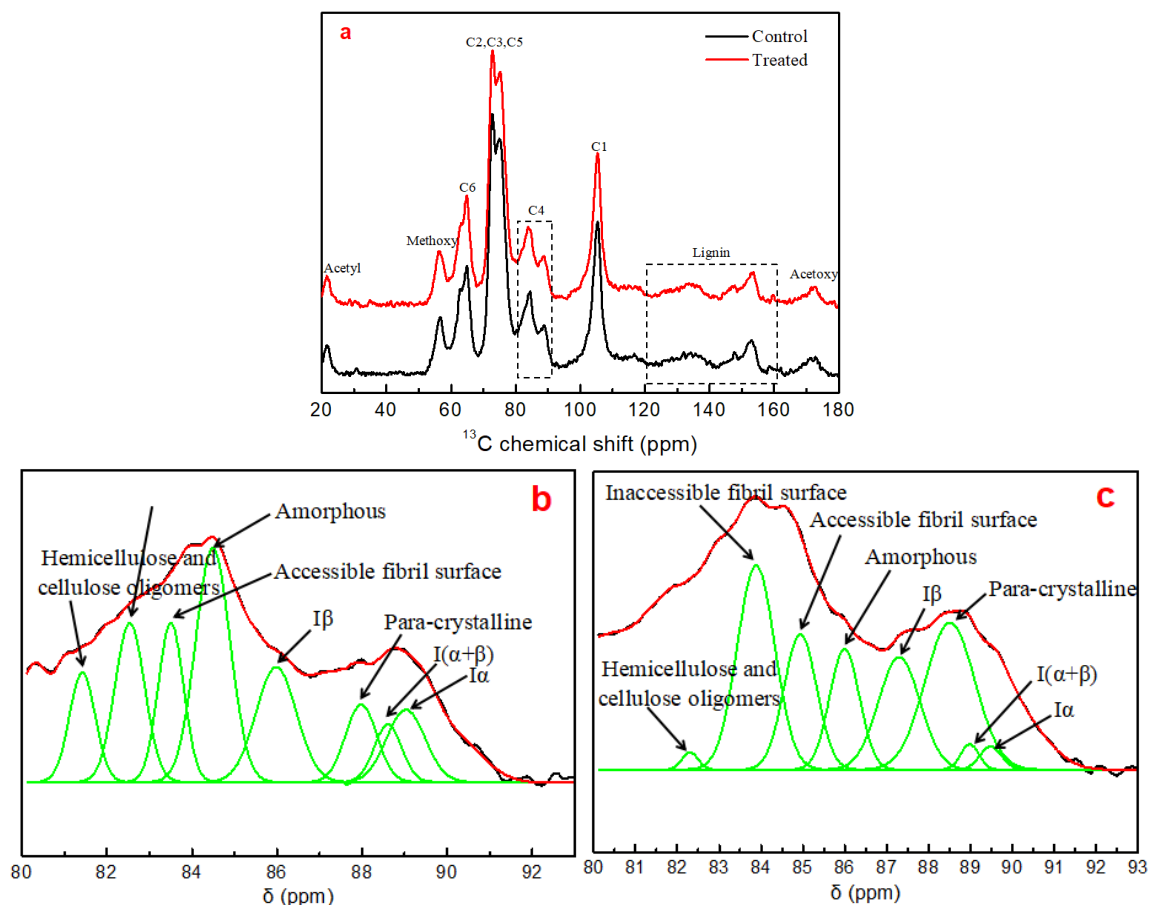


Fig. 6. The CP/MAS ^{13}C NMR spectra of the samples (a) and the result of the fitting of C4 region for cellulose from control bamboo (b) and treated bamboo (c)

NMR Analysis

The solid-state NMR spectra and fitted plots of the C4 region, shown in Fig. 6, were used for comparison of the treated bamboo samples. Figure 6a shows the main chemical composition and spectrum of the acetyl group. The signal intensity weakened obviously at 22 ppm, indicating that the hemicellulose had been partially degraded under microwave irradiation. At the same time, the signal intensity also decreased at 56 and 72 ppm, mainly showing the reductions in the anomeric C6 and polysaccharides in the treated samples (Guo *et al.* 2019). The signal intensity in treated bamboo stems was reduced to 55-58 ppm due to methoxy deoxygenation in lignin (Javed *et al.* 2015). The signal at 117 ppm was attributed to the aromatic hydroxyl groups of lignin (Tjeerdsma *et al.* 1998), which decreased slightly after microwave drying. Absorbance peaks at 153 and 148 ppm represent non-phenolic and phenolic syringyl groups, and the change in the structure of β -O-4 was a reflection of the change in the ratio of the two. The stronger absorbance peak at 148 ppm indicated the destruction of the β -O-4 structure. In addition, the acid group signals of acetyl carbon and hemicellulose were weakened at 173 ppm, indicating that they were partially degraded under microwave treatment. The signal at 81~90 ppm was attributed to C4, mainly due to the crystalline and amorphous regions of cellulose (Larsson *et al.* 1997). The C4 region was fitted with a Gaussian method to reveal any chemical shifts of the treated bamboo samples (Fig. 6b and 6c).

Table 1 lists the chemical principal shifts. The treated samples showed a decreasing trend in the amorphous regions, near-fibrous surfaces, and hemicellulose.

Table 1. The Fitting Results of C4 Region from Samples by CP/MAS ^{13}C NMR

Sample	Assignment	δ (ppm)	Intensity (%)	FWHM	Peak type
Control	Cellulose I α	89.46	2.82	0.97	Gauss
	Cellulose I(α + β)	89.02	5.40	1.06	Gauss
	Para-crystalline	88.60	3.05	0.75	Gauss
	Cellulose I β	87.97	4.71	0.87	Gauss
	Amorphous	85.98	9.00	1.11	Gauss
	Accessible fibril surface	84.49	15.56	0.95	Gauss
	Inaccessible fibril surface	83.50	7.79	0.70	Gauss
	Hemicellulose and cellulose oligomers	82.53	9.13	0.82	Gauss
	Hemicellulose	81.94	4.02	0.61	Gauss
	Treated	Cellulose I α	89.48	0.85	0.62
Cellulose I(α + β)		88.98	0.77	0.51	Gauss
Para-crystalline		88.51	12.24	1.39	Gauss
Cellulose I β		87.29	7.84	1.17	Gauss
Amorphous		85.99	6.02	0.83	Gauss
Accessible fibril surface		84.93	7.42	0.91	Gauss
Inaccessible fibril surface		83.88	12.90	1.05	Gauss
Hemicellulose and cellulose oligomers		82.30	0.47	0.45	Gauss
Hemicellulose		81.92	1.58	0.61	Gauss

The hydrogen bonds on the surface of bamboo were induced by microwave treatment during dehydration and condensation, and the internal hydrogen bond structure became more stable. The hydrophobicity and dimensional stability of bamboo were thus enhanced (Zhang *et al.* 2021). Therefore, while the amorphous region decreased, the subcrystalline fibers were enhanced under microwave conditions. In addition, the partial

decomposition of hemicellulose produced acetic acid. This was consistent with the FTIR results. In addition, I α cellulose was converted to I β cellulose, resulting in a decrease in I α and an increase in I β during microwave treatment. Since cellulose reflects strength and hemicellulose reflects elasticity, increasing crystallinity and decreasing hemicellulose increased the dimensional stability of bamboo and increased the mechanical strength of bamboo (Lv *et al.* 2018).

CONCLUSIONS

1. The treated samples showed a smoother surface, and the treatment method had no significantly adverse effects on fiber cell walls. The parenchyma cells were slightly deformed after microwave treatment, and the wall layers and of the internal surface remained clearly visible. The small-angle X-ray scattering analysis revealed that the porosity of the structure increased during microwave treatment. Besides, more microfibrils were exposed and aggregated on the surface of cell wall. The space taken by hydroxyl groups was reduced and more hydrogen bonds formed. The uniformity of the microfibrils was improved. The relative peak intensity at 3440 cm⁻¹, assigned to surface O-H stretching, decreased after microwave treatment. The main decreases in peak intensity were attributed to the degradation of hemicellulose, polysaccharides, and the cleavage of acetyl chains. Meanwhile, more intermolecular and intramolecular bonds were formed, which made the arrangement of microfibrils more consistent, creating a smoother surface.
2. Raman spectroscopy showed there was a condensation reaction involving pairs of adjacent surface hydroxyl groups under microwave conditions and revealed the formation of intramolecular hydroxyl groups in the amorphous region, both of which contributed to increasing the consistency of the fiber arrangement. The opposite trend occurred at 1600 cm⁻¹, which was similar to the weakening trend in the stretching vibration peak at 1450 cm⁻¹, indicating that the fractions of HCH and HOC bonds in aromatic skeleton decreased. The ester bonds between lignin and hemicellulose were broken by microwave treatment. The methoxy and aromatic ring hydroxyl groups were oxidized, as demonstrated by the increase in the absorption peak at 148 ppm. The amorphous region near the fiber surface and hemicellulose content decreased, but there was an increase in the secondary crystalline fibers.
3. Overall, the results suggest that microwave drying of round bamboo could be applied at an industrial scale.

ACKNOWLEDGMENTS

This work was supported by the National Natural Science Foundation of China (32230072) and (32101601). Undergraduate Innovation and Entrepreneurship Training program of Anhui Agricultural University (X202210364254).

REFERENCES CITED

- Anita, S. H., Solihat, N. N., Sari, F. P., Risanto, L., Fatriasari, W., and Hermiati, E. (2020). "Optimization of microwave-assisted oxalic acid pretreatment of oil palm empty fruit bunch for production of fermentable sugars," *Waste and Biomass Valorization* 11(6), 2673-2687. DOI: 10.1007/s12649-018-00566-w
- Atalla, R. H., and Agarwal, U. P. (1985). "Raman microprobe evidence for lignin orientation in the cell walls of native woody tissue," *Science* 227, 636-638. DOI: 10.1126/science.227.4687.636
- Belt, T., Keplinger, T., Hänninen, T., and Rautkari, L. (2017). "Cellular level distributions of Scots pine heartwood and knot heartwood extractives revealed by Raman spectroscopy imaging," *Industrial Crops and Products* 108, 327-335. DOI: 10.1016/j.indcrop.2017.06.056
- Bock, P., and Gierlinger, N. (2019). "Infrared and Raman spectra of lignin substructures: Coniferyl alcohol, abietin, and coniferyl aldehyde," *Journal of Raman Spectroscopy* 50(6), 778-792. DOI: 10.1002/jrs.5588
- Casdorff, K., Keplinger, T., Rüggeberg, M., and Burgert, I. (2018). "A close-up view of the wood cell wall ultrastructure and its mechanics at different cutting angles by atomic force microscopy," *Planta* 247(5), 1123-1132. DOI: 10.1007/s00425-018-2850-9
- Chen, H., Wu, J., Shi, J., Zhang, W., and Wang, H. (2021). "Effect of alkali treatment on microstructure and thermal stability of parenchyma cell compared with bamboo fiber," *Industrial Crops and Products* 164, article 113380. DOI: 10.1016/j.indcrop.2021.113380
- Elbaum, R., Zaltzman, L., Burgert, I., Fratzl, P. (2007). The role of wheat awns in the seed dispersal unit," *Science* 316, 884-886. DOI: 10.1126/science.1140097.
- Emmanuel, V., Odile, B., and Celine, R. (2015). "FTIR spectroscopy of woods: A new approach to study the weathering of the carving face of a sculpture," *Spectrochimica Acta Part A: Molecular and Biomolecular Spectroscopy* 136, 1255-1259. DOI: 10.1016/j.saa.2014.10.011
- Fatriasari, W., Anita, S. H., and Risanto, L. (2017). "Microwave assisted acid pretreatment of oil palm empty fruit bunches (EFB) to enhance its fermentable sugar production," *Waste and Biomass Valorization* 8(2), 379-391. DOI: 10.1007/s12649-016-9573-6
- Felhofer, M., Bock, P., Singh, A. Prats-Mateu, B., Zirbs, R., and Gierlinger, N. (2020). "Wood deformation leads to rearrangement of molecules at the nanoscale," *Nano Letter* 20, 2647-2653. DOI: 10.1021/acs.nanolett.0c00205
- Grantham, N. J., Wurman-Rodrich, J., Terrett, O. M., Lyczakowski, J. J., Stott, K., Iuga, D., Simmons, T. J., Durand-Tardif, M., Brown, S. P., Dupree, R., *et al.* (2017). "An even pattern of xylan substitution is critical for interaction with cellulose in plant cell walls," *Nature Plant* 3, 859-865. DOI: 10.1038/s41477-017-0030-8
- Guo, J., Xiao, L., Han, L., Wu, H., Yang, T., Wu, S., and Yin, Y. (2019). "Deterioration of the cell wall in waterlogged wooden archeological artifacts, 2400 years old," *IWA Journal* 40(4), 820-844. DOI: 10.1163/22941932-40190241
- Hanus, J., and Mazeau, K. (2006). "The xyloglucan-cellulose assembly at the atomic scale," *Biopolymers: Original Research on Biomolecules* 82(1), 59-73. DOI: 10.1002/bip.20460

- Huang, X., Kocaefe, D., Kocaefe, Y., Boluk, Y., and Krouse, C. (2013). "Structural analysis of heat-treated birch (*Betula papyrifera*) surface during artificial weathering," *Appl. Surf. Sci.* 264, 117-127. DOI: 10.1016/j.apsusc.2012.09.137
- Javed, M. A., Kekkonen, P. M., Ahola, S., and Telkki, V.-V. (2015). "Magnetic resonance imaging study of water absorption in thermally modified pine wood," *Holzforschung* 69(7), 899-907. DOI: 10.1515/hf-2014-0183
- Jiang, Z. H. (2007). *Bamboo and Rattan in the World*, China Forestry Pub. House, Beijing.
- Kalutskaya, E. P., and Gusev, S. S. (1980). "An infrared spectroscopic investigation of the hydration of cellulose," *Polymer Science USSR* 22(3), 550-556. DOI: 10.1016/0032-3950(80)90378-0
- Kang, X., Kirui, A., Dickwella Widanage, M., Mentink-Vigier, F., Cosgrove, D., Wang, T. (2019). "Lignin-polysaccharide interactions in plant secondary cell walls revealed by solid-state NMR," *Nature Communication* 10, 1-9. DOI: 10.1038/s41467-018-08252-0.
- Khalil, H. P. S. A., Bhat, I. U. H., Jawaid, M., Zaidon, A., Hermawan, D., and Hadi, Y. S. (2012). "Bamboo fibre reinforced biocomposites: A review," *Materials & Design* 42, 353-368. DOI: 10.1016/j.matdes.2012.06.015
- Larsson, P. T., Wickholm, K., and Iversen, T. (1997). "A CP/MAS¹³C NMR investigation of molecular ordering in celluloses," *Carbohydrate Research* 302(1-2), 19-25. DOI: 10.1016/S0008-6215(97)00130-4
- Li, Z., Chen, C., Xie, H., Yao, Y., Zhang, X., Brozena, A., Li, J., Ding, Y., Zhao, X., Hong, M., et al. (2022). "Sustainable high-strength macrofibres extracted from natural bamboo," *Nature Sustainability* 5(3), 235-244. DOI: 10.1038/s41893-021-00831-2
- Lian, C., Chen, H., Zhang, S., Liu, R., Wu, Z., and Fei, B. (2021). "Characterization of ground parenchyma cells in Moso bamboo (*Phyllostachys edulis*-Poaceae)," *IAWA Journal* 43(1-2), 92-102. DOI: 10.1163/22941932-bja10076
- Lin, Q., Liu, S., Wang, X., Huang, Y., and Yu, W. (2022). "Preparation of ultra-conductive bamboo cellulose fiber via a facile pretreatment," *Applied Surface Science* 575, article 151700. DOI: 10.1016/j.apsusc.2021.151700
- Lv, H., Chen, M., Ma, X., Li, J., Zhang, B., Fang, C., and Fei, B. (2018). "Effects of different drying methods on bamboo's physical and mechanical properties," *Forest Products Journal* 68(4), 445-451. DOI: 10.13073/FPJ-D-18-00009
- Lv, H., Chen, X., Liu, X., Fang, C., Liu, H., Zhang, B., and Fei, B. (2018). "The vacuum-assisted microwave drying of round bamboos: Drying kinetics, color and mechanical property," *Materials Letters* 223, 159-162. DOI: 10.1016/j.matlet.2018.04.038
- Lv, H., Wang, Y., Qu, M., Zhang, Y., Song, Z., Su, X., and Xu, B. (2022). "Anti-fungal activity of *Dalbergia retusa* extract on *Gloeophyllum trabeum*," *Frontiers in Plant Science* 13, article 2065. DOI: 10.3389/fpls.2022.906041
- Mood, S. H., Golfeshan, A. H., Tabatabaei, M., Jouzani, G. S., Najafi, G. H., Gholami, M., and Ardjmand, M. (2013). "Lignocellulosic biomass to bioethanol, a comprehensive review with a focus on pretreatment," *Renewable and Sustainable Energy Reviews* 27, 77-93. DOI: 10.1016/j.rser.2013.06.033
- Ozgenç, O., Durmaz, B., Boyacı, I. K., and Eksi-Kocak, H. (2017). "Determination of chemical changes in heat-treated wood using ATR-FTIR and FT Raman spectrometry," *Spectrochimica Acta Part A Mol. Biomol. Spectrosc.* 171, 395-400. DOI: 10.1016/j.saa.2016.08.026

- Parameswaran, N., and Liese, W. (1976). "On the fine structure of bamboo fibres," *Wood Science and Technology* 10(4), 231-246. DOI: 10.1007/BF00350830
- Peng, Y., Gardner, D. J., and Han, Y. (2012). "Drying cellulose nanofibrils: In search of a suitable method," *Cellulose* 19(1), 91-102. DOI: 10.1007/s10570-011-9630-z
- Prasad, B. E., and Pandey, K. K. (2012). "Microwave drying of bamboo," *European Journal of Wood and Wood Products* 70(1), 353-355. DOI: 10.1007/s00107-010-0496-9
- Prats Mateu, B., Hauser, M. T., Heredia, A., and Gierlinger, N. (2016). "Waterproofing in Arabidopsis: Following phenolics and lipids *in situ* by confocal Raman microscopy," *Frontiers in Chemistry* 4, article 10. DOI: 10.3389/fchem.2016.00010
- Schwan, J., Ulrich, S., Batori, V., and Ehrhardt, H. (1996). "Raman spectroscopy on amorphous carbon films," *Journal of Applied Physics* 80(1), 440-447. DOI: 10.1063/1.362745
- Shen, X. J., Wen, J. L., Mei, Q. Q., Chen, X., Sun, D., Yuan, T. Q., and Sun, R. C. (2019). "Facile fractionation of lignocelluloses by biomass-derived deep eutectic solvent (DES) pretreatment for cellulose enzymatic hydrolysis and lignin valorization," *Green Chemistry* 21, 275-283. DOI: 10.1039/C8GC03064B
- Tjeerdsmas, B. F., Boonstra, M., Pizzi, A., Tekely, P., and Militz, H. (1998). "Characterisation of thermally modified wood: Molecular reasons for wood performance improvement," *Holz als Roh-und Werkstoff* 56(3), 149-153. DOI: 10.1007/s001070050287
- Toscan, A., Morais, A. R. C., Paixão, S. M., Alves, L., Andreus, J., Camassola, M., Pinheiro Dillon, A. J., and Lukasik, R. M. (2017). "Effective extraction of lignin from elephant grass using imidazole and its effect on enzymatic saccharification to produce fermentable sugars," *Industrial & Engineering Chemistry Research* 56(17), 5138-5145. DOI: 10.1021/acs.iecr.6b04932
- Tsubaki, S., Oono, K., Onda, A., Yanagisawa, K., and Azuma, J. I. (2013). "Comparative decomposition kinetics of neutral monosaccharides by microwave and induction heating treatments," *Carbohydrate Research* 375, 1-4. DOI: 10.1016/j.carres.2013.04.013
- Wang, X., Liu, J., Shi, F., Liu, S., Feng, X., and Bao, L. (2014). "Influences of heat-treatment on the microstructure and properties of silica-titania composite aerogels," *Journal of Porous Materials* 21(3), 293-301. DOI: 10.1007/s10934-013-9774-3
- Wang, H. M., Wang, B., Wen, J. L., Yuan, T. Q., and Sun, R. C. (2017). "Structural characteristics of lignin macromolecules from different Eucalyptus species," *ACS Sustainable Chemistry & Engineering* 5(12), 11618-11627. DOI: 10.1021/acssuschemeng.7b02970
- Wu, Y. Q. (2021). "Newly advances in wood science and technology," *Journal of Central South University of Forestry & Technology* 41(01), 1-28.
- Yan, Y., Fei, B., and Liu, S. (2022). "The relationship between moisture content and shrinkage strain in the process of bamboo air seasoning and cracking," *Dry Technology* 40, 571-580. DOI: 10.1080/07373937.2020.1819307.
- Zhang, S., Lin, Q., Wang, X., Yu, Y., Yu, W., and Huang, Y. (2022). "Bamboo cellulose fibers prepared by different drying methods: Structure-property relationships," *Carbohydrate Polymers* 296, article 119926. DOI: 10.1016/j.carbpol.2022.119926

- Zhang, X., Li, J., Yu, Z., Yu, Y., Wang, H. (2017). “Compressive failure mechanism and buckling analysis of the graded hierarchical bamboo structure,” *Journal of materials Science* 52, 6999-7007. DOI: doi.org/10.1007/s10853-017-0933-9.
- Zhang, Y., Yu, Y., Lu, Y., Yu, W., and Wang, S. (2021). “Effects of heat treatment on surface physicochemical properties and sorption behavior of bamboo (*Phyllostachys edulis*),” *Construction and Building Materials* 282, article 122683. DOI: 10.1016/j.conbuildmat.2021.122683
- Zhou, X., Wang, P., Zhang, Y., Lulu Wang, L., Zhang, L., Zhang, L., Xu, L., and Liu, L. (2017). “Biomass based nitrogen-doped structure-tunable versatile porous carbon materials,” *Journal of Materials Chemistry A* 5(25), 12958-12968. DOI: 10.1039/C7TA02113E

Article submitted: January 16, 2023; Peer review completed: February 4, 2023; Revised version received and accepted: April 16, 2023; Published: April 24, 2023.
DOI: 10.15376/biores.18.2.4071-4084